

Article

Axial confocal tomography of capillary-contained colloidal structures.

Shir R Liber, Ganit Indech, Ernest Benjamin Van der Wee, Alexander V. Butenko, Thomas E Kodger, Peter James Lu, Andrew B. Schofield, David A. Weitz, Alfons van Blaaderen, and Eli Sloutskin

Langmuir, **Just Accepted Manuscript** • DOI: 10.1021/acs.langmuir.7b03039 • Publication Date (Web): 18 Oct 2017

Downloaded from <http://pubs.acs.org> on October 19, 2017

Just Accepted

"Just Accepted" manuscripts have been peer-reviewed and accepted for publication. They are posted online prior to technical editing, formatting for publication and author proofing. The American Chemical Society provides "Just Accepted" as a free service to the research community to expedite the dissemination of scientific material as soon as possible after acceptance. "Just Accepted" manuscripts appear in full in PDF format accompanied by an HTML abstract. "Just Accepted" manuscripts have been fully peer reviewed, but should not be considered the official version of record. They are accessible to all readers and citable by the Digital Object Identifier (DOI®). "Just Accepted" is an optional service offered to authors. Therefore, the "Just Accepted" Web site may not include all articles that will be published in the journal. After a manuscript is technically edited and formatted, it will be removed from the "Just Accepted" Web site and published as an ASAP article. Note that technical editing may introduce minor changes to the manuscript text and/or graphics which could affect content, and all legal disclaimers and ethical guidelines that apply to the journal pertain. ACS cannot be held responsible for errors or consequences arising from the use of information contained in these "Just Accepted" manuscripts.



ACS Publications

Langmuir is published by the American Chemical Society, 1155 Sixteenth Street N.W., Washington, DC 20036

Published by American Chemical Society. Copyright © American Chemical Society. However, no copyright claim is made to original U.S. Government works, or works produced by employees of any Commonwealth realm Crown government in the course of their duties.

Axial confocal tomography of capillary-contained colloidal structures

Shir R. Liber,^{†,⊥} Ganit Indech,^{†,⊥} Ernest B. van der Wee,[‡] Alexander V. Butenko,[†] Thomas E. Kodger,[¶] Peter J. Lu,[§] Andrew B. Schofield,^{||} David A. Weitz,[§] Alfons van Blaaderen,[‡] and Eli Sloutskin^{*,†}

Physics Dept. and Institute of Nanotechnology, Bar-Ilan University, Ramat-Gan 5290002, Israel, Soft Condensed Matter, Debye Institute for NanoMaterials Science, Utrecht University, Princetonplein 1, 3584 CC, Utrecht, The Netherlands, Physical Chemistry and Soft Matter, Wageningen University & Research, Stippeneng 4, 6708 WE Wageningen, The Netherlands, Department of Physics and SEAS, Harvard University, Cambridge, Massachusetts 02138, USA, and The School of Physics and Astronomy, University of Edinburgh, Edinburgh EH9 3FD, UK

E-mail: eli.sloutskin@biu.ac.il

Abstract

Confocal microscopy is widely used for three-dimensional (3D) sample reconstructions. Arguably, the most significant challenge in such reconstructions is posed by the

^{*}To whom correspondence should be addressed
[†]Physics Dept. and Institute of Nanotechnology, Bar-Ilan University, Ramat-Gan 5290002, Israel
[‡]Soft Condensed Matter, Debye Institute for NanoMaterials Science, Utrecht University, Princetonplein 1, 3584 CC, Utrecht, The Netherlands
[¶]Physical Chemistry and Soft Matter, Wageningen University & Research, Stippeneng 4, 6708 WE Wageningen, The Netherlands
[§]Department of Physics and SEAS, Harvard University, Cambridge, Massachusetts 02138, USA
^{||}The School of Physics and Astronomy, University of Edinburgh, Edinburgh EH9 3FD, UK
[⊥]Contributed equally to this work

resolution along the optical axis being significantly lower than in the lateral directions. In addition, the imaging rate is lower along the optical axis in most confocal architectures, prohibiting reliable 3D reconstruction of dynamic samples. Here we demonstrate a very simple, cheap, and generic method of multiangle microscopy, allowing high resolution high-rate confocal slice collection to be carried out with capillary-contained colloidal samples, in a wide range of slice orientations. This method, realizable with any common confocal architecture and recently implemented with macroscopic specimens enclosed in rotatable cylindrical capillaries, allows 3D reconstructions of colloidal structures to be verified by direct experiments and provides a solid testing ground for complex reconstruction algorithms. In this paper, we focus on the implementation of this method for dense non-rotatable colloidal samples, contained in complex shape capillaries. Additionally, we discuss strategies to minimize potential pitfalls of this method, such as the artificial appearance of chain-like particle structures.

Introduction

Confocal microscopy is one of the central tools in modern soft condensed matter physics, chemistry, biology, and material science.¹ The optical sectioning capabilities of confocal microscopy, with the spatial resolution within each slice approaching the diffraction limit, make full three dimensional (3D) structural reconstructions possible, providing an unprecedentedly detailed insight into the physics of collective phenomena in colloidal suspensions^{2,3} and resolving the full geometry of complex shape micro-objects,^{4,5} such as the recently discovered faceted liquid emulsion droplets.⁶ Typically, the individual optical cross sections are collected by scanning the fluorescently-stained sample with (one or multiple) laser beam(s), exciting fluorophores. This in-plane scanning may be very fast, commonly carried out at super-video rates. To take confocal sections at varying depths inside the sample, either the objective or the sample are translated along the optical axis. This on-axis scanning is typically slower and less accurate, limiting most confocal studies of dynamical systems to imaging of a single

section normal to the optical axis; thus, the full 3D information is only available for systems exhibiting relatively slow dynamics. In these quasi-static situations, a stack of optical slices is collected. A 3D reconstruction of such a stack commonly involves a 3D deconvolution, with the point spread function used as a kernel. The point spread function (PSF) of the confocal microscopes is rotationally anisotropic: the resolution along the optical axis is typically lower by a factor of ~ 3 compared to the other directions, along which the diffraction limit may be approached quite closely.⁷ The PSF anisotropy challenges its precise deconvolution from the confocal data, complicates feature detection,^{8–12} and limits the reliability of quantitative analysis based on these data.

In recent studies of crustaceans, ixodidae ticks, and live cells embedded in an agarose gel,^{13,14} axial rotation of the specimens, enclosed in a cylindrical capillary, was demonstrated to allow confocal slicing of the sample in multiple different directions; this axial confocal tomography (ACT) allowed the resolution for all the three spatial dimensions of the specimen to be maximized, effectively overcoming the anisotropy of the PSF.¹⁵ A similar goal was also achieved by applying optical tweezers to rotate individual bacteria under the microscope.¹⁶ However, ACT has never been applied yet to colloidal science. The implementation of ACT to colloids is challenged by the fact that some samples, such as colloidal sediments, cannot be rotated: rotation with respect to the direction of gravity changes their structure. Also, samples exhibiting long range particle correlations are sensitive to the shape of the enclosing capillary; embedding these samples in a cylindrical capillary may alter their behavior. Thus, confocal reconstructions of colloidal structures are based on complex numerical algorithms;^{8–12,17,18} some peculiar inaccuracies of such algorithms remain hidden for decades, in spite of their very active employment by many groups worldwide.^{8,19,20} Solid testing grounds, which may be provided by ACT for such algorithms, are essential for colloidal science.

In this paper, we apply ACT to fluid suspensions and solid non-crystalline sediments of colloidal spheres. We extend the ACT method to samples which cannot be rotated and to non-cylindrical capillaries. We identify the potential pitfalls of this method and demonstrate

1
2
3 how these pitfalls may be avoided. While our work focuses on colloids, these extensions of
4 ACT also contribute to other fields of science where specimen fixation for axial rotation is
5 challenging. Moreover, similar methods may be applied in combination with 2D stimulated
6 emission depletion (STED) where the lateral resolution is reduced to < 50 nm, while the
7 resolution along the optical axis remains similar to confocal microscopy.²¹ Although the
8 extension of STED into the axial direction does enable a spherical PSF,²² the combination
9 of 2D STED and axial tomography remains more powerful, resulting in a smaller PSF in
10 all directions. Thus, some of the remarkable recent success of TEM (transmission electron
11 microscopy) tomography^{23,24} may possibly be achieved by ACT and other similar optical
12 tomography techniques, with the potentially destructive sample freezing/drying completely
13 avoided and beam damages practically eliminated.

25 26 27 28 29 30 31 32 33 34 35 36 37 38 39 40 41 42 43 44 45 46 47 48 49 50 51 52 53 54 55 56 57 58 59 60

We apply the ACT method to both apolar and polar colloidal suspensions. For the apolar (or low-polar) suspensions, we use PMMA [poly-(methymethacrylate)] spheres, fluorescently-labelled for confocal imaging by either DiIC₁₈ (1,1'-dioctadecyl-3,3,3',3'-tetramethylindotricarbocyanine iodide), NBD (7-nitro-1,2,3-benzoxadiazole), rhodamine B isothiocyanate, or the Nile Red dye.^{2,11,19,20,25–27} To form fluid suspensions, these particles were suspended in buoyancy-matched tetrachloroethylene:decahydronaphthalene (TCE:DHN) and bromocyclohexane:decahydronaphthalene mixtures, where mixed decahydronaphthalene was used. These mixtures roughly match the refractive index of the particles ($n_{\text{ap01}} \approx 1.49$); thus, light scattering is weak, allowing the confocal imaging to be carried out at depths > 100 μm into the bulk of the suspensions. A more precise index matching was achieved, where necessary, by introducing tetrahydronaphthalene into these solvent combinations^{20,28,29} and replacing mixed DHN by a pure cis-DHN. To prepare colloidal sediments, PMMA particles were centrifuged (3000 *ref*), in either a pure decahydronaphthalene or a decahydronaphtha-

lene:tetrahydronaphthalene mixture. The dielectric constants of all the above-mentioned solvent combinations are in the 2 – 6 range, too low for the dissolution of most common salts; thus, micron-scale Debye length are common.^{3,29–31} The PMMA particles were sterically stabilized by PHSA [poly-(hydroxystearic) acid], which minimizes the van der Waals attractions.^{25,30} Particle diameters σ ranged from 1.5 to 6 μm .

For polar suspensions, we employed the recently-devised³² poly(trifluoroethyl methacrylate-*co*-*t*-butyl methacrylate) (PTFEMA:PtBMA) colloids, fluorescently labeled with pyromethene 546 (aka BODIPY 493; Exciton, Inc. Dayton, US) and suspended in a density- and index-matching mixture of formamide and sulfolane. The dielectric constant of this mixture is $\epsilon \approx 82$, close to that of the pure water. Sodium chloride (30 mM) was dissolved in this mixture for screening of electrostatic interactions. Two particle diameters were tested: 1.9 and 2.4 μm ; the results were essentially the same, for both particle sizes.

The suspensions were loaded into rectangular or cylindrical, borosilicate or fused silica VitrocomTM capillaries, widely used in the colloidal community and beyond, and sealed with Devcon 5 minuteTM Epoxy glue. The imaging was carried out with a laser-scanning confocal fluorescence microscope (Nikon TiE-based A1R), exciting with $\lambda = 514$ nm and scanning in either the galvanometric or the resonant mode. Imaging with the VisitechTM Vt-Infinity3 multipoint-scanning microscope led to similar results. For rapid scanning along the optical axis (with either confocal setup), the objective was mounted on a PI (P-725.2CL) piezo stage. For confocal imaging of samples contained in rectangular capillaries, the capillaries were fixed at the edge of an L-shaped construction, made of two supporting glass slides. Two different orientations of the capillary with respect to the microscope sample stage, are possible with such a construction. For the ACT data to be collected over a continuous range of $> 200^\circ$, the samples were loaded into cylindrical VitrocomTM borosilicate capillaries ($ID = 0.1$ mm) and the configurations shown in Fig. 1(a)-(b) were used. The capillaries were mounted on a U-shape aluminum capillary holder (visible in Fig. 1(b)). For samples which could be rotated with respect to gravity, this holder was mounted on a D-8219 HuberTM

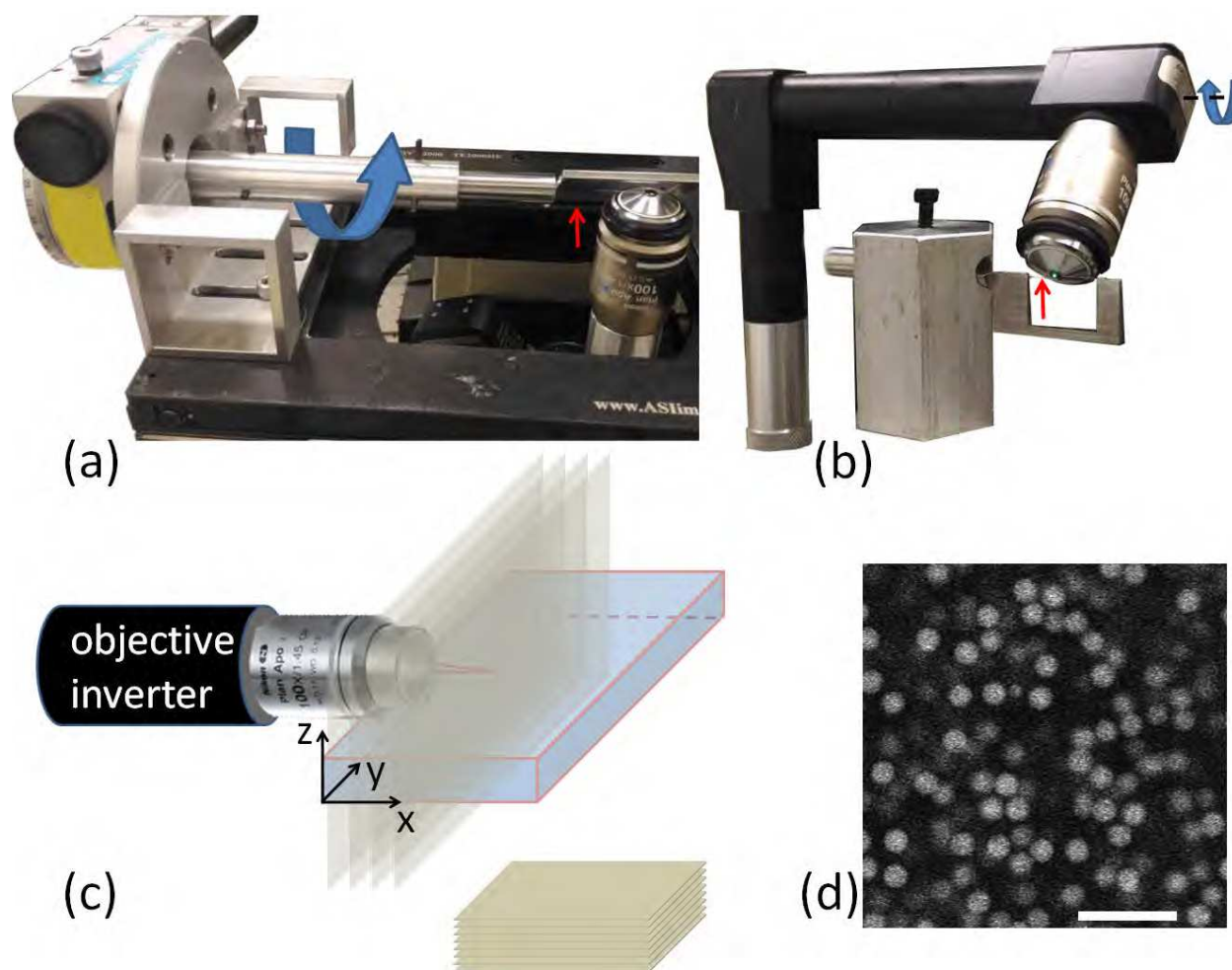


Figure 1: (a) Axial confocal tomography (ACT) setup allowing slices in a wide range of sample orientations to be collected for rotatable samples, contained in a cylindrical capillary (marked by a red arrow). The sample is rotated about the long axis of the capillary and translated in the horizontal plane employing a combination of a rotation stage and a translation stage. The distance between the sample and the objective is controlled by the microscope nosepiece. (b) ACT of non-rotatable samples, contained in cylindrical capillaries, requires the optical axis to be rotated by an objective inverter. Here sample translation in all three spatial dimensions is enabled; the translation range of a typical nosepiece is too short for the ACT measurements in a wide angular range to be carried out. The sample containing capillary is marked by a red arrow. Dashes mark the rotation axis of the objective inverter. (c) For a rectangular capillary, only two different orientations of the optical axis are possible; here the optical axis is horizontal (marked in red). The classical orientation of the confocal slices is shown at the bottom. (d) A typical confocal slice of a colloidal suspension, obtained with the optical axis aligned along the gravitational direction and along the z axis of the rectangular capillary. Note that the particles are isotropically distributed and no particle chains are visible. The scale bar length is $10\ \mu\text{m}$.

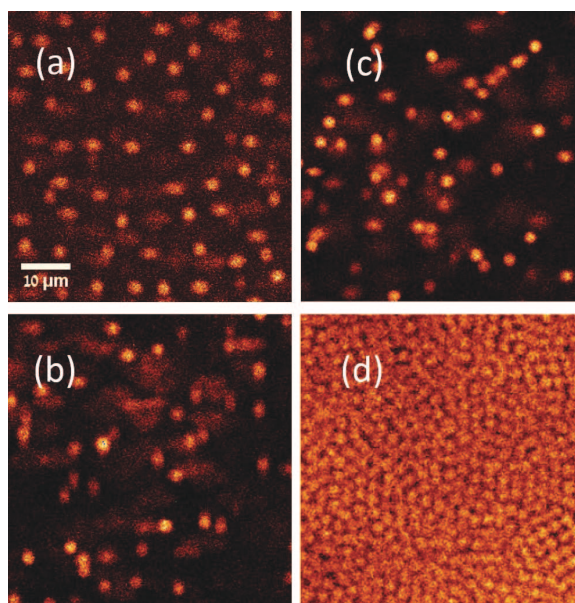


Figure 2: Vertical ACT yz -slices taken through the colloidal fluids allow the rotational isotropy of these systems to be confirmed, providing a benchmark for the classical 3D confocal reconstruction algorithms. (a) PMMA particles density- and index-matched in a TCE:DHN mixture. Note, this yz -slice through the fluid appears isotropic, akin to the xy - slice shown in Fig. 1(d). (b) To optimize the quality of the ACT images, an accurate matching of the refractive indices of all optical elements downstream of the objective is necessary, as achieved here for the PTFEMA:PtBMA suspension. In particular, the slight aberration-induced smearing of PMMA colloids in (a), is completely eliminated here. Changing from fused silica (b) to borosilicate (c) capillary does not strongly deteriorate the optical quality, as long as the immersion fluid is index-matched with the capillary wall. (d) For fully index-matched suspensions of PTFEMA:PtBMA, even the high-density solid colloidal sediments, prepared by settling in a centrifuge, appear perfectly isotropic, further emphasizing the ACT capabilities.

rotation stage (Fig. 1(a)), allowing the capillary to be rotated about its long axis with an accuracy of 0.01° . The rotation stage was mounted onto the MS-2000 ASITM stage, for horizontal translation. For full ACT of non-rotatable samples, we fixed the capillary holder directly to the horizontal translation stage, with this stage itself mounted on top of a vertical translation stage. For imaging of non-rotatable samples, contained in either the rectangular (Fig. 1(c)) or the cylindrical (Fig. 1(b)) capillaries, we used an InverterScope[®] objective inverter from LSM Tech, which is a simple periscope, allowing the optical axis to be rotated in any spatial direction. The rotation axis employed in our work is marked in Fig. 1(b). We graduated the inverter for rotations about this axis (the current graduation allows for a

1
2
3 resolution of 3.75°). A 100x Nikon Plan Apo VC or λ oil immersion objective (NA=1.4 and
4 1.45, respectively) was mounted on top of the objective inverter (Fig. 1(b)-(c)). When the
5 optical axis is at angle with the vertical (i.e., the scanning axis of the microscope's nosepiece),
6 the images appear rotated by that angle. To eliminate this effect where necessary, we carried
7 back-rotation by a standard ImageJ procedure.
8
9

10
11 The ray tracing calculations, employing geometrical optics, were carried out with a ded-
12 icated MatlabTM code. The wave front of the illuminating radiation is numerically approx-
13 imated by $\sim 10^4$ separate rays, aiming towards a common focal point inside the sample.
14 The rays refract, according to the Snell's law, at the external and the internal interfaces of
15 a cylindrical capillary. We neglect multiple reflection phenomena and the dependence of the
16 reflected and refracted intensities on the angle of incidence. The chromatic dispersion is also
17 neglected.
18
19

20 21 22 23 24 25 26 27 28 29 30 31 32 33 34 35 36 37 38 39 40 41 42 43 44 45 46 47 48 49 50 51 52 53 54 55 56 57 58 59 60

As a test case for the ACT method, we employ a fluid suspension of PMMA colloidal spheres
in a density- and index- matching TCE:DHN mixture. Earlier experiments demonstrated
that the bulk structures of similar suspensions are closely matched by the hard spheres'
theoretical model,^{2,19} indicating that the van der Waals attractions and the charge effects
are very small.^{30,33} Indeed, in confocal slices taken through the wide wall of the rectangular
VitrocomTM, the suspension looks isotropic and disordered like a simple fluid of hard spheres
(Fig. 1(d)). To reconstruct the 3D structure of the fluid by one of the common classical
procedures,¹⁰ we collected a 3D stack of such slices. The slice separation was $\sim 0.1\sigma$, where
 σ is the particle diameter. With the particle centers in all slices located,¹⁹ we use the fact
that each particle is visible in ~ 10 different cross sections to evaluate the full 3D coordinates
of its center.¹⁰ While more advanced algorithms, treating the positioning along all the three
axes equally and evaluating the PSF have been proposed,^{8,12} their implementation remains

quite challenging even with the modern computer architectures. Therefore, the 'linking' of particle cross sections' centers to locate its 3D center position is widely used in colloidal studies; however, the strong anisotropy of the PSF, distorting particle shapes, challenges both the linking process and its testing by comparison to the raw 3D confocal data. In particular, the tracked 3D particle centers imply that the distribution of nearest neighbors $P(\theta, \phi)$ about each particle is rotationally anisotropic, peaking along the optical axis (Fig. S1). The peak to peak variation of $P(\theta, \phi)$ strongly depends on the details of the linking algorithm and on the involved parameter values, commonly exceeding 20%; peaks in the focal plane may occur as well, depending on the subtleties of the linking algorithm. The observed shape of $P(\theta, \phi)$ suggests z -oriented chains to be formed within these samples, breaking the fluid rotational symmetry (see Fig. 1(c) for the geometry).

To directly test the validity of our 3D-linking, we employ the ACT, confocally-slicing the sample with the optical axis kept parallel to the x -axis of the capillary, as in Fig. 1(c). To avoid optical refraction at the complex-shape side walls of the VitrocomTM borosilicate capillaries, potentially inducing complex lensing effects, we immerse the objective in an aqueous mixture of glycerol, which closely matches the refractive index of borosilicate. As expected, the ACT images of this sample, for all cross section orientations, are perfectly isotropic: no chain formation can be discerned (Fig. 2(a)). Thus, the apparent anisotropy of $P(\theta, \phi)$ owes to possible inaccuracies of the 3D particle linking procedure.

With the isotropy of our fluids confirmed by ACT, we use these fluids to improve the accuracy of the particle linking algorithms. In particular, we noticed that an increased sensitivity of some of the 3D reconstruction algorithms to fluctuations of particle intensity between the subsequent confocal slices may occasionally result in particle double counting.¹⁰ The duplicated particles thus produced, form short chains aligned along the optical axis, giving rise to the artificial anisotropy of $P(\theta, \phi)$. This artifact is readily eliminated by neglecting intensity fluctuations below a certain threshold, demonstrating the advantage of the ACT for quality control of 3D reconstructions (Fig. S1). While only homogeneously-labeled

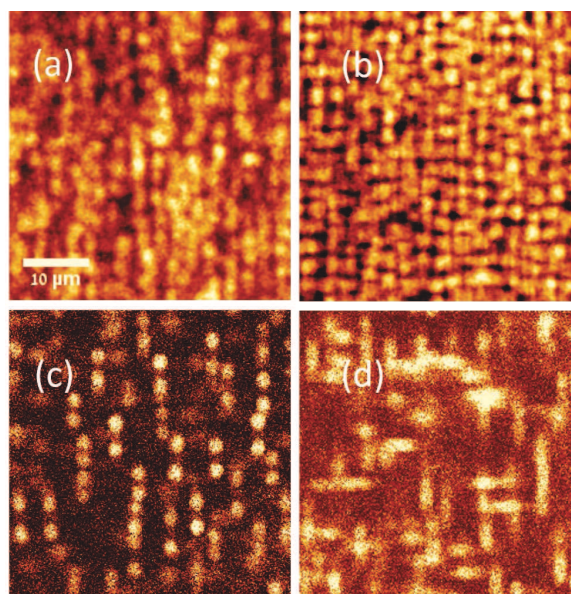


Figure 3: Artificial particle chains in 'side-view' ACT images of colloidal suspensions. These confocal cross sections were obtained through the narrow (yz -) wall of the rectangular $0.1 \times 2 \times 50$ mm borosilicate VitrocomTM capillaries, with the Nikon type A oil used for objective immersion. (a) A dense fluid of PMMA colloids in a density- and index- matching TCE:DHN solvent exhibits z -aligned artificial chains (see also Supplementary Video 3). (b) The chains appear in solid sediments of the same particles, as well. Compare to Fig. 2(d), where a similar sediment is shown to be completely isotropic. (c) Larger intra-chain particle separations occur in dilute suspensions, as if the particles repel by electrostatics. (d) These artificial chains, born by light refraction at the walls of the capillary, are visible even for the polar suspensions, where $\epsilon \approx 82$ and significant ion concentrations are present. With the intra-chain particle separations far exceeding the Debye length, chain formation cannot be attributed to the electrostatic interactions.

colloids are used in our current work, the 3D reconstruction precision is also improved for core-shell colloids, where only the cores are fluorescent and the optically-transparent shells allow for a better feature separation in optical microscopy;³⁴ however, the synthesis of the core-shell particles is more involved. Notably, while only four different ACT slice orientations are possible for rectangular capillaries, cylindrical capillaries allow for a continuum of slice orientations, providing a great wealth of data. Thus, the parameters of 3D linking algorithms can be fine-tuned, achieving high-accuracy 3D reconstructions with either the homogeneously-labeled or the core-shell particles.

A further improvement to the optical quality of the ACT slices is achieved by match-

ing the refractive indices of all the optical components. Instead of the PMMA particles ($n_{\text{ap01}} \approx 1.49$), deviating in their refractive index from the VitrocomTM capillaries, we employ PTFEMA:PtBMA colloids, suspended in a mixture of formamide and sulfolane. We introduce this polar suspension into a fused silica rectangular VitrocomTM capillary and closely match both the refractive index of the suspension ($n_{\text{po1}} = 1.45$) and that of the capillary ($n_{\text{fs}} = 1.46$) by an immersion liquid composed of water and glycerol ($n_{\text{wg}} = 1.45$). The ACT images of this sample, for all cross section orientations, are still perfectly isotropic (Fig. 2(b)). Remarkably, the slight optical aberrations which distorted the PMMA colloids' appearance in Fig. 2(a), do not occur for the PTFEMA:PtBMA (Fig. 2(b)), demonstrating the importance of having all scattering and refraction effects eliminated by the index matching. Indeed, the aberrations reemerge when the fused silica capillary is replaced by a borosilicate one ($n_{\text{bs}} = 1.47$, Fig. 2(c)).

With the scattering and refraction minimized, ACT can readily be applied to samples at much higher particle densities. In particular, we obtain a yz - ACT slice through a solid random packing of PTFEMA:PtBMA colloids (Fig 2(d)), where the particle volume fraction is $\varphi \approx 0.6$;² note the excellent image quality. Accurate classical 3D confocal reconstructions are increasingly challenging at high φ , which further emphasizes the benefits of the ACT.

While only a few different optical axis orientations are possible with the rectangular capillaries, a wide and continuous range of such orientations is accessible for samples contained in cylindrical capillaries. For rotatable samples contained in cylindrical capillaries, we employ the setup in Fig. 1(a) to demonstrate imaging of the same sample region over a range of different directions (Fig. S2 and Video 1). For non-rotatable samples, we rotate the optical axis, while the sample is translated with no rotation (Fig. 1(b)). Again, a wide range of imaging orientations is possible, as demonstrated in Video 2. Advanced algorithms for in-parallel particle location in confocal image stacks taken from different angles of observation are currently under development. These algorithms, potentially allowing for a much greater precision in particle location, should not require tremendously large computational resources

or an *a priori* knowledge of the PSF.^{8,12}

While refractive index variation across the sample deteriorates the image quality as shown, much more dramatic artifacts occur in ACT when the refractive index of the immersion fluid mismatches that of the capillary wall. These effects are quite subtle and also occur in some other situations, where imaging through curved interfaces is involved;³⁵ thus, we discuss these artifacts in some detail. In particular, while the xy -slices through the PMMA suspensions appear isotropic (Fig. 1(d)), a significant structuring appears in the yz -slices, when obtained with the type A immersion oil ($n_A = 1.52$) for suspensions contained in the borosilicate capillaries (Fig. 3(a)). These apparent chains fluctuate and diffuse around, as demonstrated in Supplementary Video 3. The chains only appear at relatively large depths into the bulk of the sample ($x > 50 \mu\text{m}$); closer to the capillary wall, the fluid looks much more isotropic. The chains' appearance is independent of sample orientation with respect to gravity; thus, chain formation is not a result of a (possible) small deviation from perfect neutral-buoyancy. The chains exist at different φ , with the excess probability for z -aligned nearest-neighbor bonds monotonically decreasing with φ . Yet, these artificial chains are clearly visible even at an ultra-high $\varphi \approx 0.6$, in a solid amorphous sediment² of these colloids (Fig. 3(b)). This artifact is not sensitive to the particularities of the particle synthesis, appearing for different PMMA particle batches and also for colloids with a covalently-linked fluorescent dye, 'heat-shocked' for rapid equilibration with the solvent²⁷ (see Fig. S3). In low- φ fluids, the intra-chain particle spacing is increased (Fig. 3(c) and Supplementary Video 4). This apparent long range of intra-chain particle repulsions, as also chains' alignment with respect to the capillary walls, are not an electrostatic effect, contrasting with the true physical chains formed by external AC electric fields in similar suspensions.^{31,36} Indeed, the electrostatics should be tunable by colloid and solvent charge regulation, commonly achieved by the introduction of TBAC (tetrabutylammonium chloride) or AOT (dioctyl sulfosuccinate sodium surfactant) micelles into the suspension.³⁷⁻³⁹ As expected, no systematic variation of either the artificial chain alignment or the intra-chain

particle spacing is detected with the introduction of AOT or TBAC at various concentrations, even when conductivities exceed $1\mu\text{S}/\text{m}$. The corresponding sub- μm Debye lengths are much smaller than the distance between the apparent chains and the capillary walls. It is even smaller than the intra-chain particle separation. Evidently, electrostatic interactions in common polar solvents cannot exceed the Debye length by so much. While the electrostatics of the *apolar* solvents at ultra-low charge concentrations is yet not well established,^{38,39} similar chains are visible also in the *polar* PTFEMA:PtBMA suspensions, where the Debye length (at 30mM NaCl) $< 2\text{ nm}$ is precisely known (Fig. 3(d)).

While clearly not of an electrostatic origin, the artificial chains' alignment along the z -axis of the sample-containing capillary suggests that the container plays an important role in chain formation. Indeed, we see no chains in capillaries with square (0.5×0.5 and $0.6 \times 0.6\text{ mm}$) cross sections. Also, no chains form in a cuvette ($\sim 0.1 \times 2 \times 2\text{ mm}$), prepared by carefully gluing together several standard fused silica or borosilicate microscopy cover slips. Since changing the objective immersion oil from type A ($n_{\text{A}} = 1.52$) to a glycerol-water mixture ($n_{\text{WG}} = 1.45$) eliminates the artificial structuring of the fluid (Fig. 2(a)), we conclude that the apparent chains are resulted by a complex lensing effect along the z -axis of the rectangular VitrocomTM capillaries, which significantly distorts the optical image in z -direction.

For the details of this lensing mechanism to be fully resolved, the exact shape and thickness profile of the rectangular capillary side walls must be known. This profile is not available from the manufacturer and is also challenging to measure. However, a similar artificial chain formation effect is also detected for capillaries with a rounded cross section, 0.6 mm in internal diameter, where the geometry is simpler. We trace the optical rays refracted at the 0.12 mm -thick walls of such a capillary, with the type A oil used for the objective immersion. In our case, the refraction at the capillary walls dominates optical distortions; therefore, for simplicity, we only use geometrical optics and neglect other aberration sources. Under the settings considered, for a flat 0.12 mm -thick coverslip, the optical rays emanate from the $100\times$

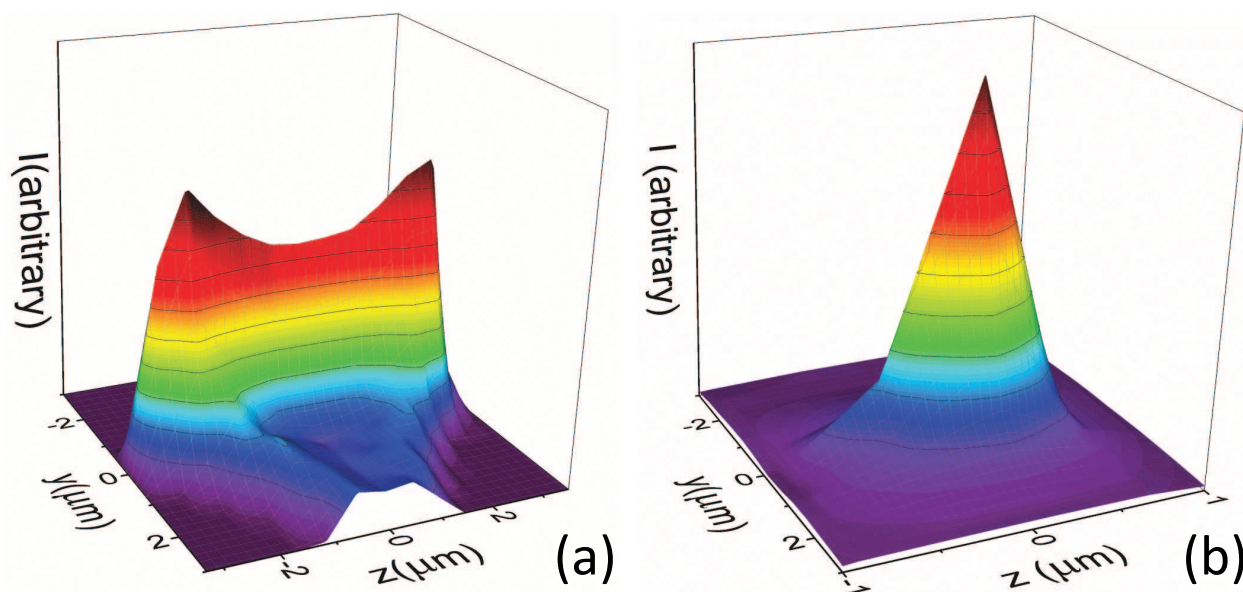


Figure 4: Ray tracing calculations demonstrate that the curvature of side walls in cylindrical capillaries gives rise to a splitting of the focal point. (a) Rays emanating from the objective towards a single focal point at a depth of $60\ \mu\text{m}$, refract at the capillary wall. As a result, the rays split in two groups, each of which intersects at a different location, giving rise to splitting of the focus. The two peaks of the intensity I correspond to the locations of the two foci in a yz -cross-section of the sample, $56\ \mu\text{m}$ from the capillary wall. Here the refractive index of the suspension is $n_{\text{apo1}} = 1.49$, and the type A ($n_{\text{A}} = 1.52$) immersion oil is used with fused silica capillaries. (b) Repeating the same calculation with the type A immersion oil replaced by a glycerol:water mixture ($n_{\text{WG}} = 1.45$), yields only a single focus (at a depth of $64\ \mu\text{m}$); thus, no artificial chains are expected to form. This prediction is fully corroborated by experiment (Fig. 2). Note, the different z scale in (a) and (b), further emphasizing the sharpness of the single focal point shown in (b).

objective ($\text{NA}=1.4$), propagating inside the immersion fluid towards a single focal point, at a distance of $60\ \mu\text{m}$ into the bulk of the suspension ($n_{\text{apo1}} = 1.49$). However, when the coverslip is replaced by a rounded capillary wall, the rays do not intersect at an individual location inside the sample. Instead, two separate focal points are clearly visible, as demonstrated in Fig. 4(a). The duplication of foci along the z -axis of the capillary (Fig. 1(c)) gives rise to an artificial formation of z -oriented particle pairs, as in Fig. 3(c): each such pair is simply a duplicated image of an individual particle. The focal points are separated by $\sim 4\ \mu\text{m}$, in a good agreement with the experimentally-detected intra-chain particle spacing. A similar phenomenon has been very recently detected in light-sheet microscopy images of very dilute

colloids ($\varphi \rightarrow 0$), enclosed in cylindrical capillaries.⁴⁰

To experimentally confirm that the particle chains are formed by an artifactual multiplication of individual particle images, we prepare a binary mixture of PMMA particles of two different sizes. An artificial chain formed by optical image multiplication must ultimately consist of one particle size only: no mixed chains of small and large particles can form by this mechanism. This prediction is fully corroborated by our experiment. All experimentally-detected chains consist of only one type of particles: no mixed chains are observed (see Supplementary Video 5). This experiment provides a clear-cut evidence that the chains are formed by an optical artifact, in agreement with our ray tracing. In addition, we also confirm this result by particle counting: average particle densities in the yz -slices obtained through the side wall of the rectangular capillaries are higher than in the xy -slices, obtained through the bottom.

To completely avoid the optical ACT artifacts discussed above, the refractive indices of all the components of the optical path must be matched. Ideally, the refractive index of the objective should be matched to the other components as well. In particular, a glycerol objective, equipped by a correction ring to compensate for index variations between 1.447 and 1.455, is commercially available and may be used for the PTFEMA:PtBMA system, as also for silica colloids (see Fig. S4). Clearly, such matching is impossible for most samples and particularly where the studied specimens are natural, rather than synthetic. However, our ray tracing calculations demonstrate that the refraction-induced splitting of foci may be eliminated, once the refractive index of the immersion fluid matches that of the capillary wall. For example, for the apolar PMMA suspension, replacing the type A immersion fluid by the capillary-matching glycerol:water mixture eliminates focal splitting, in spite of the refractive index of this suspension $n_{\text{apol}} = 1.49$ being mismatched with other components of the optical path (cf. Fig. 4(b) and (a)). Other types of aberration may be present in such index-mismatched optical configurations, but commonly these are less dramatic than the formation of particle chains. Indeed, replacing the immersion fluid in our experimental

1
2
3 ACT of apolar PMMA suspensions completely eliminated the artificial chains (cf. Fig. 2(a)
4 and Fig. 3(c)), as predicted by ray tracing calculations.
5
6
7
8

9 10 Conclusions

11
12 In axial confocal tomography (ACT), the orientation of the confocal point spread function is
13 varied relative to the sample, so that the highest optical resolution is achieved in all three di-
14 mensions. We have realized ACT with colloidal samples in a wide range of particle densities.
15 The necessary measures to avoid the optical artifacts in such experiments were thoroughly
16 discussed. In particular, index-matching of the curved capillary walls by immersion liquid
17 was shown to be crucial, for the artifactual duplication of particle images to be avoided. We
18 have demonstrated the ACT to set a benchmark for testing of the 3D reconstruction algo-
19 rithms, allowing their accuracy and reliability to be significantly improved. In the future, the
20 demonstrated ACT of samples slowly rotated in cylindrical capillaries may also be employed
21 to mimic effective microgravity conditions of a high current interest in colloidal community
22 and beyond.⁴¹
23
24
25
26
27
28
29
30
31
32
33
34
35
36

37 Acknowledgement

38
39 The authors are grateful to Y. Rabin, D. Osmanović, A. Nikolaenkova, M. Hermes and
40 W. Vlug for fruitful discussions, to M. Izoh, G. Gershinsky and P. Helfferich for technical
41 assistance, and to the Kahn foundation for the purchase of equipment. Acknowledgment is
42 made by SRL, GI, AVB, and ES to the donors of the American Chemical Society Petroleum
43 Research Fund for support of this research. PJJ and DAW thank NASA (NNX13AQ48G)
44 for the financial support. AvB and EBvdW acknowledge the European Research Council
45 (ERC) under the European Union's Seventh Framework Programme (FP/2007-2013)/ERC
46 Grant Agreement 291667.
47
48
49
50
51
52
53
54
55
56
57
58
59
60

Supporting Information Available

Video files (1-5) and the corresponding captions, as also supplementary figures Fig. S1-S4, with captions. This material is available free of charge via the Internet at <http://pubs.acs.org/>.

References

- (1) Conchello, J. A.; Lichtman, J.W. Optical Sectioning Microscopy. *Nat. Methods* **2005**, *2*, 920-931.
- (2) Liber, S. R.; Borohovich, S.; Butenko, A. V.; Schofield, A. B.; Sloutskin, E. Dense Colloidal Fluids Form Denser Amorphous Sediments. *Proc. Natl. Acad. Sci. USA* **2013**, *110*, 5769-5773.
- (3) Cohen, A. P.; Dorosz, S.; Schofield, A. B.; Schilling, T.; Sloutskin E. Structural Transition in a Fluid of Spheroids: A Low-Density Vestige of Jamming. *Phys. Rev. Lett.* **2016**, *116*, 098001.
- (4) Kuijk, A; Imhof, A; Verkuijlen, M. H. W.; Besseling, T. H.; van Eck, E. R. H.; van Blaaderen, A. Colloidal Silica Rods: Material Properties and Fluorescent Labeling. *Part. Part. Syst. Char.* **2014**, *31*, 706-713.
- (5) Besseling, T. H.; Hermes, M.; Kuijk, A.; de Nijs, B.; Deng, T. S.; Dijkstra, M.; Imhof, A.; van Blaaderen, A. Determination of the Positions and Orientations of Concentrated Rod-Like Colloids from 3D Microscopy Data. *J. Phys.: Condens. Matter* **2015**, *27*, 194109.
- (6) Guttman, S.; Sapir, Z.; Schultz, M.; Butenko, A. V.; Ocko, B. M.; Deutsch, M.; Sloutskin, E. How Faceted Liquid Droplets Grow Tails. *Proc. Natl. Acad. Sci. USA* **2016**, *113*, 493-496.

- (7) Besseling, T. H.; Jose, J.; van Blaaderen, A. Methods to Calibrate and Scale Axial Distances in Confocal Microscopy as a Function of Refractive Index. *J. Microsc.* **2015**, *257*, 142-150.
- (8) Leocmach, M.; Tanaka, H. A Novel Particle Tracking Method with Individual Particle Size Measurement and its Application to Ordering in Glassy Hard Sphere Colloids. *Soft Matter* **2013**, *9*, 1447-1457.
- (9) van Blaaderen, A.; Wiltzius, P. Real-Space Structure of Colloidal Hard-Sphere Glasses. *Science* **1995**, *270*, 1177-1179.
- (10) Lu, P. J.; Sims, P. A.; Oki, H.; Macarthur, J. B.; Weitz, D. A. Target-Locking Acquisition with Real-Time Confocal (TARC) Microscopy. *Opt. Express*. **2007**, *15*, 8702-8712.
- (11) Dinsmore, A. D.; Weeks, E. R.; Prasad, V.; Levitt, A. C.; Weitz, D. A. Three-Dimensional Confocal Microscopy of Colloids. *Appl. Opt.* **2001**, *40*, 4152-4159.
- (12) Bierbaum, M.; Leahy, B. D.; Alemi, A. A.; Cohen, I.; Sethna, J. P. Light Microscopy at Maximal Precision. arXiv:1702.07336 [cond-mat.soft] **2017**.
- (13) Bruns, T.; Schickinger, S.; Schneckenburger, H. Sample Holder for Axial Rotation of Specimens in 3D Microscopy. *J. Microsc.* **2015**, *260*, 30-36.
- (14) Richter, V.; Bruns, S.; Bruns, T.; Weber, P.; Wagner, M.; Cremer, C.; Schneckenburger, H. Axial Tomography in Live Cell Laser Microscopy. *J. Biomed. Opt.* **2017**, *22*, 091505.
- (15) Heintzmann, R.; Cremer, C. Axial Tomographic Confocal Fluorescence Microscopy. *J. Microsc.* **2002**, *206*, 7-23.
- (16) Carmon, G.; Kumar, P.; Feingold, M. Optical Tweezers Assisted Imaging of the Z-Ring in *Escherichia Coli*: Measuring Its Radial Width. *New J. Phys.* **2014**, *16*, 013043.
- (17) Crocker, J. C.; Grier, D. J. Methods of Digital Video Microscopy for Colloidal Studies. *J. Colloid Interface Sci.* **1996**, *179*, 298-310.

- (18) Dassanayake, U.; Fraden, S.; van Blaaderen, A. Structure of Electrorheological Fluids. *J. Chem. Phys.* **2000**, *112*, 3851-3858.
- (19) Lu, P. J.; Shutman, M.; Sloutskin, E.; Butenko, A. V. Locating Particles Accurately in Microscope Images Requires Image-Processing Kernels to be Rotationally Symmetric. *Opt. Express* **2013**, *21*, 30755-30763.
- (20) Gao, Y.; Kilfoil, M. L. Accurate Detection and Complete Tracking of Large Populations of Features in Three Dimensions. *Opt. Express* **2009**, *17*, 4685-4704.
- (21) Wildanger, D.; Medda, R.; Kastrup, L.; Hell, S. W. A Compact STED Microscope Providing 3D Nanoscale Resolution. *J. Microsc.* **2009**, *236*, 35-43.
- (22) Klar, T. A.; Jakobs, S.; Dyba, M.; Egner, A.; Hell, S. W. Fluorescence Microscopy with Diffraction Resolution Barrier Broken by Stimulated Emission. *Proc. Natl. Acad. Sci. USA* **2000**, *97*, 8206-8210.
- (23) de Nijs, B.; Dussi, S.; Smalenburg, F.; Meeldijk, J. D.; Groenendijk, D. J.; Filion, L.; Imhof, L.; van Blaaderen, A.; Dijkstra, M. Entropy-Driven Formation of Large Icosahedral Colloidal Clusters by Spherical Confinement. *Nat. Mater.* **2015**, *14*, 56-60.
- (24) Zanaga, D.; Bleichrodt, F.; Altantzis, T.; Winckelmans, N.; Palestijn, W. J.; Sijbers, J.; de Nijs, B.; van Huis, M. A.; Liz-Marzán, L. M.; van Blaaderen, A.; Batenburg, J.; Bals, S.; van Tendeloo, G. Quantitative 3D Analysis of Huge Nanoparticle Assemblies. *Nanoscale* **2016**, *8*, 292-299.
- (25) Antl, L.; Goodwin, J. W.; Hill, R. D.; Ottewill, R. H.; Owens, S. M.; Papworth, S.; Waters, J. A. The Preparation of Poly(methyl Methacrylate) Latices in Non-Aqueous Media. *Colloids Surf. A* **1986**, *17*, 67-78.
- (26) Cohen, A. P.; Alesker, M.; Schofield, A. B.; Zitoun, D.; Sloutskin, E. Photo-

- Crosslinkable Colloids: From Fluid Structure and Dynamics of Spheres to Suspensions of Ellipsoids. *Gels* **2016**, *2*, 29.
- (27) Kodger, T. E.; Lu, P. J.; Wiseman, G. R.; Weitz, D. A. Stable, Fluorescent Polymethylmethacrylate Particles for the Long-Term Observation of Slow Colloidal Dynamics. *Langmuir* **2017**, *33*, 6382-6389.
- (28) Wiederseiner, S.; Andreini, N.; Epely-Chauvin, G.; Ancey, C. Refractive-Index and Density Matching in Concentrated Particle Suspensions: a Review. *Exp. Fluids* **2011**, *50*, 1183-1206.
- (29) Cohen, A. P.; Janai, E.; Mogilko, E.; Schofield, A. B.; Sloutskin, E. Fluid Suspensions of Colloidal Ellipsoids: Direct Structural Measurements. *Phys. Rev. Lett.* **2011**, *107*, 238301.
- (30) Royall, C. P.; Poon, W. C. K.; Weeks, E. R. In Search of Colloidal Hard Spheres. *Soft Matter* **2013**, *9*, 17-27.
- (31) Yethiraj, A.; van Blaaderen, A. A Colloidal Model System with an Interaction Tunable From Hard Sphere to Soft and Dipolar. *Nature* **2003**, *421*, 513-517.
- (32) Kodger, T. E.; Guerra, R. E.; Sprakel, Precise Colloids with Tunable Interactions for Confocal Microscopy. *J. Sci. Rep.* **2015**, *5*, 14635.
- (33) Janai, E.; Cohen, A. P.; Butenko, A. V.; Schofield, A. B.; Schultz, M.; Sloutskin, E. Dipolar Colloids in Apolar Media: Direct Microscopy of Two-Dimensional Suspensions. *Sci. Rep.* **2016**, *6*, 28578.
- (34) Klein, M. K.; Saenger, N. R.; Schuetter, S.; Pfeiderer, P.; Zumbusch, A. Shape-Tunable Core-Shell Microparticles. *Langmuir* **2014**, *30*, 12457-12464.
- (35) Elbers, N. A.; van der Hoeven, J. E. S.; de Winter, D. A. M.; Schneijdenberg, C. T. W. M.; van der Linden, M. N.; Fillion, L.; van Blaaderen, A. Repulsive van der Waals

- Forces Enable Pickering Emulsions with Non-Touching Colloids. *Soft Matter* **2016**, *12*, 7265-7272.
- (36) Crassous, J. J.; Mihut, A. M.; Wernersson, E.; Pfeleiderer, P.; Vermant, J.; Linse, P.; Schurtenberger, P. Field-Induced Assembly of Colloidal Ellipsoids into Well-Defined Microtubules. *Nat. Commun.* **2014**, *5*, 5516.
- (37) Hsu, M. F.; Dufresne, E. R.; Weitz, D. A. Charge Stabilization in Nonpolar Solvents. *Langmuir* **2005**, *21*, 4881-4887.
- (38) Smith, G. N.; Eastoe, J. Controlling Colloid Charge in Nonpolar Liquids with Surfactants. *Phys. Chem. Chem. Phys.* **2013**, *15*, 424-439.
- (39) Kemp, R.; Sanchez, R.; Mutch, K. J.; Bartlett, P. Nanoparticle Charge Control in Nonpolar Liquids: Insights from Small-Angle Neutron Scattering and Microelectrophoresis. *Langmuir* **2010**, *26*, 6967-6976.
- (40) Meinert, T.; Gutwein, B. A.; Rohrbach, A. Light-Sheet Microscopy in a Glass Capillary: Feedback Holographic Control for Illumination Beam Correction. *Opt. Lett.* **2017**, *42*, 350-353.
- (41) El Masri, D.; Vissers, T.; Badaire, S.; Stiefelhagen, J. C. P.; Vutukuri, H. R.; Helfferich, P.; Zhang, T. H.; Kegel, W. K.; Imhof, A.; van Blaaderen, A. A Qualitative Confocal Microscopy Study on a Range of Colloidal Processes by Simulating Microgravity Conditions through Slow Rotations. *Soft Matter* **2012**, *8*, 6979-6990.

Graphical TOC Entry

